

---

# LP-SFT: LOCAL-PRESERVING SUPERVISED FINE-TUNING VIA MULTIMODAL ENTROPY STRUCTURE \*

---

Yueyang Wang<sup>1†</sup> Baolong Bi<sup>2</sup> Shuo Lu<sup>3</sup> Jingyuan Zhang<sup>4</sup>

<sup>1</sup>School of Mathematical Sciences, Peking University

<sup>2</sup>Institute of Computing Technology, Chinese Academy of Sciences

<sup>3</sup>Institute of Automation, Chinese Academy of Sciences

<sup>4</sup>College of Computing, Georgia Institute of Technology

## ABSTRACT

Supervised fine-tuning (SFT) is the standard approach for adapting pretrained language models to downstream domains, yet it often improves target-domain behavior at the cost of degrading pre-existing capabilities. Standard cross-entropy fine-tuning promotes only the observed label token and leaves unconstrained how probability mass is redistributed over other plausible alternatives, potentially distorting the rich local preference structure learned during pretraining. We first analyze next-token predictions using Shannon and Rényi entropies, revealing that pretrained models exhibit a regular multimodal entropy structure. These entropy peaks correspond to varying numbers of plausible alternatives, indicating that the base model intrinsically encodes rich distributional knowledge beyond the single supervised token. Motivated by this observation, we propose **LP-SFT**, a **Local-Preserving Supervised Fine-Tuning** objective designed to explicitly protect this inherent entropy structure. At each step, LP-SFT constructs an adaptive support of alternative tokens and applies a locally normalized preservation loss to maintain the base model’s relative structure among them, while standard cross-entropy independently optimizes the supervised token. Across mixed-domain and single-domain fine-tuning experiments, LP-SFT improves overall performance over vanilla SFT and recent SFT-enhancement baselines, achieving the best balance between pass@1 accuracy and pass@ $k$  performance. These results suggest that local preservation helps mitigate capability degradation without collapsing sampling-accessible diversity.

**Keywords** Supervised Fine-Tuning · Catastrophic Forgetting · Distribution Preservation · Multimodal Entropy Structure

## 1 Introduction

Supervised fine-tuning (SFT) has become the dominant paradigm for adapting pretrained language models to instruction following, reasoning, coding, and domain-specific tasks[16, 18]. Despite its simplicity and effectiveness, SFT often induces capability degradation along two dimensions: over-specialization to the fine-tuning distribution, which can cause catastrophic forgetting of out-of-domain capabilities, and reduced generation diversity[21], where improved single-sample accuracy may come at the cost of suppressing alternative valid solutions[15].

We argue that a significant portion of this degradation stems from the mismatch between the standard cross-entropy objective and the rich distributional knowledge encoded in pretrained models. Large language models acquire broad capabilities from diverse pretraining corpora, resulting in next-token distributions that contain substantial information beyond the single observed target token. However, cross-entropy supervises each position using only this target token, encouraging the model to fit the fine-tuning data while largely ignoring

---

\*Code is available at <https://github.com/Wakaka161/LP-SFT>.

†Corresponding author: wangyueyang@stu.pku.edu.cn

the remaining preference structure of the base distribution. Under distribution shift between pretraining and fine-tuning data, repeatedly suppressing plausible alternatives can distort this pretrained structural integrity, leading to catastrophic forgetting and reduced generation diversity.

This perspective suggests that effective fine-tuning should not only align the model with supervised targets, but also preserve useful local structure in the pretrained distribution. To understand where such preservation is most needed, we examine the entropy of next-token predictions in both base and instruction-tuned models, with particular focus on the base distribution used as the preservation reference. We find that the entropy distribution exhibits a distinct multimodal structure, with peaks near  $\ln k$  for integers  $k$ , and that this structure persists across model variants. This suggests that token positions naturally fall into discrete uncertainty regimes: some positions are nearly deterministic, while others admit a small set of plausible alternatives. Therefore, the information encoded by the base model is highly heterogeneous across token positions. Treating all tokens uniformly under standard cross-entropy may unnecessarily distort this heterogeneous structure, motivating an adaptive preservation strategy during fine-tuning.

To address this issue, we propose **LP-SFT (Local-Preserving Supervised Fine-Tuning)**, which uses the frozen base model as a local structural reference during fine-tuning. Rather than relying solely on cross-entropy, LP-SFT constructs an adaptive preservation set of alternative tokens from the base model’s next-token distribution. Guided by the entropy structure of the base distribution, LP-SFT determines how many plausible alternatives should be preserved at each token position. It then removes the supervised target token  $y_t$  from this set to avoid conflict with the cross-entropy objective, and applies a locally normalized KL loss. Crucially, this local normalization ensures that LP-SFT preserves the underlying relative structure among these alternatives without artificially constraining their absolute probability mass. In this way, LP-SFT decouples target-token learning from local structure preservation, reducing unnecessary distortion of the pretrained distribution while improving single-sample accuracy and maintaining sampling-accessible diversity.

Our contributions are summarized as follows:

- We provide a novel analysis of next-token distributions in pretrained language models and show that their entropy exhibits a distinct multimodal structure, revealing heterogeneous uncertainty regimes across token positions.
- Motivated by this observation, we propose **LP-SFT**, a local-preserving fine-tuning framework that removes the supervised token from an adaptive preservation set and uses locally normalized KL divergence to preserve relative structure among plausible non-label alternatives.
- Extensive experiments demonstrate that LP-SFT achieves a better trade-off between downstream adaptation and capability retention than vanilla SFT and recent SFT-enhancement methods, improving overall performance across pass@1 and pass@ $k$  metrics while maintaining sampling-accessible diversity.

## 2 Related Work

**Improved SFT Objectives.** A growing line of work seeks to improve supervised fine-tuning by moving beyond the standard token-level cross-entropy loss. Dynamic Fine-Tuning (DFT) [22] dynamically rescales the token-level objective using the model-assigned probability of the target token, aiming to stabilize token-level gradient updates and improve generalization. Entropy-Adaptive Fine-Tuning (EAFT) [4] uses token-level entropy as a gating signal to distinguish uncertain examples from confident conflicts, suppressing destructive gradients on conflicting tokens. GEM [13] formulates SFT as an entropy-regularized distribution matching problem to reduce overfitting and improve generation diversity. Anchored Supervised Fine-Tuning (ASFT) [24] adds a full-vocabulary KL constraint to keep the fine-tuned model close to the base distribution, but it can be sensitive to the KL weight and requires additional base-model computation during training. Overall, these methods mainly adjust the target-token learning signal or regularize the global predictive distribution. In contrast, LP-SFT uses the frozen base model as a local reference, preserving relative preferences among selected non-label alternatives without imposing a full-vocabulary constraint.

**Entropy Structure in Next-Token Prediction.** Recent work [19] observes that the Shannon entropy of next-token distributions exhibits a multimodal structure, with peaks near  $\ln k$  for small integers  $k = 1, 2, 3$ . Since a uniform distribution over  $k$  options has entropy  $\ln k$ , these peaks correspond to states where uncertainty is spread over  $k$  similarly plausible next-token candidates, referred to as *entropy-compressed states*. Related work also shows that token-level entropy is an informative training signal: high-entropy tokens often correspond to branching points in reasoning, where multiple continuations are plausible and small changes can substantially affect the final outcome [17].

### 3 Preliminaries

Given an input prompt  $\mathbf{x}$  and a target response sequence  $\mathbf{y} = (y_1, \dots, y_T)$ , the model estimates the conditional probability of the next response token  $y_t$  given the prompt and the preceding response tokens  $\mathbf{y}_{<t} = (y_1, \dots, y_{t-1})$ . Here,  $y_t$  denotes the ground-truth response token at position  $t$ . Let  $\mathcal{V}$  denote the vocabulary. At each position  $t$ , the model outputs a next-token probability distribution  $p_t(\cdot) = p_\theta(\cdot | \mathbf{x}, \mathbf{y}_{<t})$  over  $\mathcal{V}$ .

**Top- $k$  Candidate Set.** We define the top- $k$  candidate set as

$$C_k(p_t) = \{v_t^{(1)}, v_t^{(2)}, \dots, v_t^{(k)}\}, \quad (1)$$

where  $v_t^{(i)}$  denotes the token with the  $i$ -th highest probability under  $p_t$  at position  $t$ . These tokens are sorted in descending order:  $p_t(v_t^{(1)}) \geq p_t(v_t^{(2)}) \geq \dots \geq p_t(v_t^{(k)})$ .

**Top- $K$  Normalized Distribution.** For entropy analysis, we use a fixed top- $K$  truncation window and normalize the probability mass within  $C_K(p_t)$ . Unless otherwise specified, we set  $K = 30$ . The normalized probability of the  $i$ -th ranked token is

$$\hat{p}_{t,i} = \frac{p_t(v_t^{(i)})}{\sum_{j=1}^K p_t(v_t^{(j)})}, \quad i \in \{1, \dots, K\}. \quad (2)$$

**Top- $K$  Shannon Entropy.** To measure the overall uncertainty within the normalized top- $K$  distribution, we define the Shannon entropy  $H_1$  and its effective support size  $N_1$  [9, 11] as

$$H_1(p_t) = - \sum_{i=1}^K \hat{p}_{t,i} \ln \hat{p}_{t,i}, \quad N_1(p_t) = \exp(H_1(p_t)). \quad (3)$$

The effective support size  $N_1$  can be interpreted as the equivalent number of uniformly likely candidate tokens. Shannon entropy captures the overall spread of probability mass across the normalized top- $K$  candidate set.

**Top- $K$  Rényi-2 Entropy.** We also use the Rényi-2 entropy, or collision entropy, to characterize concentration among high-probability candidates. Its effective support size  $N_2$  is defined as

$$H_2(p_t) = - \ln \sum_{i=1}^K \hat{p}_{t,i}^2, \quad N_2(p_t) = \exp(H_2(p_t)) = \frac{1}{\sum_{i=1}^K \hat{p}_{t,i}^2}. \quad (4)$$

Compared with Shannon entropy, Rényi-2 entropy places more emphasis on high-probability tokens and is therefore more sensitive to concentration around dominant candidates. Throughout the paper, we use  $N_1$  and  $N_2$  to summarize the effective number of plausible next-token candidates under the normalized top- $K$  distribution.

## 4 Multimodal Entropy Structure in Next-Token Distributions

### 4.1 Effective Support Ratio for Identifying Entropy Peaks

While prior work has identified entropy-compressed states as evidence of multimodal structure in next-token prediction, existing analyses mainly characterize low-order peaks up to  $\ln 3$ , leaving higher-order entropy-compressed states insufficiently studied. To systematically identify such peaks, we introduce the *effective support ratio*. Here  $p_t$  denotes the next-token distribution of the model being analyzed, which can be either a base or instruction-tuned model:

$$R(p_t) = \frac{N_2(p_t)}{N_1(p_t)}. \quad (5)$$

Let  $\hat{p}_{t,i}$  denote the probabilities normalized over the top- $K$  tokens. The relation between  $H_1$  and  $H_2$  follows from Jensen’s inequality:

$$H_1(p_t) = - \sum_{i=1}^K \hat{p}_{t,i} \log \hat{p}_{t,i} \geq - \log \sum_{i=1}^K \hat{p}_{t,i}^2 = H_2(p_t). \quad (6)$$

Therefore,

$$R(p_t) = \frac{N_2(p_t)}{N_1(p_t)} = \exp(H_2(p_t) - H_1(p_t)) \implies 0 < R(p_t) \leq 1. \quad (7)$$

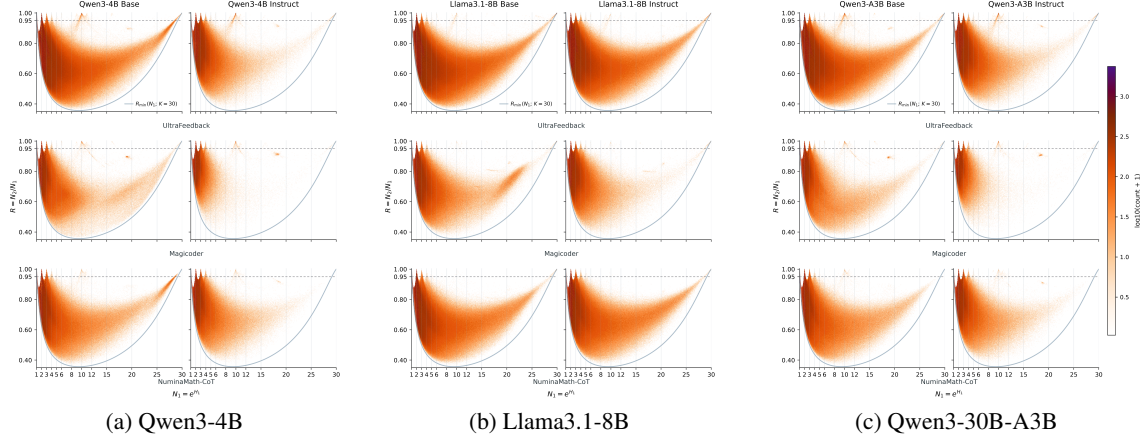


Figure 1: Joint distributions of  $N_1$  and  $R = N_2/N_1$ . High- $R$  ridges at multiple integer supports reveal higher-order entropy peaks across datasets and model families.

Since  $N_1(p_t) = \exp(H_1(p_t))$ , an entropy peak at  $H_1(p_t) \approx \ln m$  is equivalently observed as a concentration near  $N_1(p_t) \approx m$ . In the ideal plateau case where the normalized next-token distribution is uniform over  $m$  tokens, we have

$$H_1(p_t) = H_2(p_t) = \ln m, \quad N_1(p_t) = N_2(p_t) = m, \quad R(p_t) = 1. \quad (8)$$

Thus,  $N_1(p_t)$  locates the order of the entropy peak, while  $R(p_t)$  measures how close the corresponding local distribution is to a uniform plateau. A high- $R$  point with  $N_1(p_t) \approx m$  therefore indicates an entropy-compressed state with approximately  $m$  plausible next-token alternatives.

To examine whether the effective support ratio  $R$  consistently reveals the multimodal structure of next-token distributions, we compute the joint distribution of  $R$  and  $N_1$  over assistant-token positions for both base and instruction-tuned models on UltraFeedback [3], Magicoder-OSS-Instruct-75K [20], and NuminaMath-CoT [12], which represent general-domain instruction following, code generation, and mathematical reasoning, respectively. We evaluate three model families, Qwen3-4B [23], Llama3.1-8B [5], and Qwen3-30B-A3B [23], to assess whether the observed structure generalizes across different model families, architectures, and scales. We compute  $N_1$  and  $N_2$  over the normalized top- $K$  distribution with  $K = 30$ , from which  $R$  is derived.

As shown in Figure 1, the joint distribution of  $N_1$  and  $R$  exhibits clear vertical ridges near integer values of  $N_1 = 1, 2, 3, 4, 5, 10, \dots$ , especially in high- $R$  regions. These ridges indicate that the corresponding tokens lie in near-uniform entropy-compressed states with  $H_1 \approx \ln m$ , where  $m$  denotes the effective number of plausible next-token alternatives. Importantly, these ridges persist beyond the previously emphasized low-order regime, suggesting that higher-order entropy-compressed states are widespread across architectures and datasets.

**Finite-top- $K$  lower envelope.** Besides the high- $R$  ridges, Figure 1 also shows a curved lower envelope in the  $(N_1, R)$  plane. This boundary arises from the finite top- $K$  normalization used to compute  $N_1$  and  $N_2$  with  $K = 30$ . For a fixed  $N_1$ , minimizing  $R$  is equivalent to maximizing the collision probability under a fixed Shannon entropy constraint. The corresponding extremal distribution has one dominant probability and a uniform tail over an active support of size  $m$ :

$$\hat{p} = \left( q, \frac{1-q}{m-1}, \dots, \frac{1-q}{m-1}, 0, \dots, 0 \right), \quad 2 \leq m \leq K. \quad (9)$$

For this family, define

$$H_1(q, m) = -q \ln q - (1-q) \ln \frac{1-q}{m-1}. \quad (10)$$

The finite-top- $K$  lower envelope can then be written as

$$R_{\min}(N_1; K) = \min_{2 \leq m \leq K, q \in [1/m, 1]} \frac{1}{N_1 \left[ q^2 + \frac{(1-q)^2}{m-1} \right]} \quad \text{s.t.} \quad H_1(q, m) = \ln N_1. \quad (11)$$

With  $K = 30$ , this lower-envelope curve closely matches the empirical boundary in Figure 1. Intuitively, when one token dominates while the remaining probability mass is spread over many low-probability alternatives,  $N_1$  can be enlarged by the diffuse tail while  $N_2$  remains dominated by the top-1 probability, causing  $R = N_2/N_1$  to decrease in the middle regime. The full derivation is provided in Appendix A.

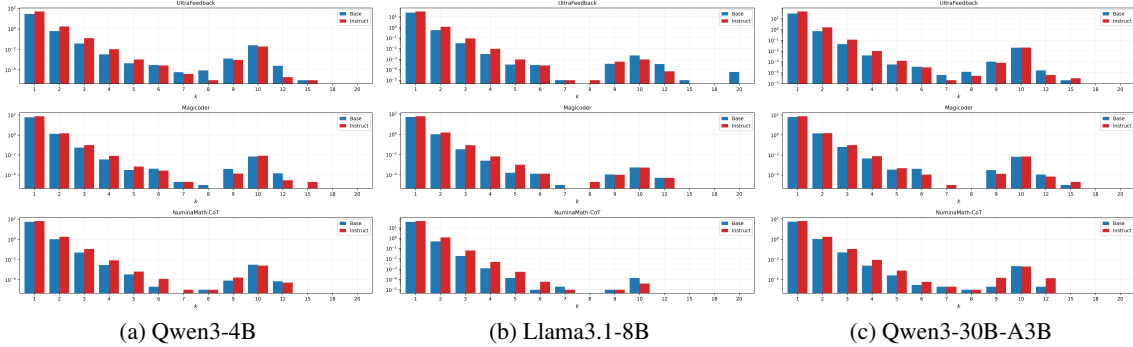


Figure 2: Occurrence of plateau- $k$  states, defined by  $N_1 \in [k - 0.3, k + 0.3]$  and  $R > 0.95$ . Instruction tuning increases low-order plateaus ( $k = 1-5$ ) while reducing or preserving higher-order plateaus ( $k > 5$ ).

## 4.2 Plateau- $k$ States: From Low-Order Branching to High-Order Ambiguity

We define entropy-compressed states of order  $k$  as plateau- $k$  states, captured by

$$N_1 \in [k - 0.3, k + 0.3] \quad \text{and} \quad R > 0.95. \tag{12}$$

Figure 2 reports the proportion of plateau- $k$  states for base and instruction-tuned models across three model families. A clear pattern emerges in the low-order regime ( $k = 1-5$ ): instruction-tuned models generally exhibit a higher proportion of plateau states than their base counterparts. In contrast, for higher-order plateaus ( $k > 5$ ), this trend is weakened or even reversed. This suggests that post-training does not merely sharpen the distribution toward plateau-1 states, where the model assigns most probability mass to a single dominant next-token candidate, but also increases the occurrence of low-order entropy-compressed states, where uncertainty is distributed over a small set of plausible alternatives. Meanwhile, the higher-order regime behaves differently, with a visible concentration around  $k = 10$ . We analyze these phenomena in more detail below, with representative examples from Qwen3-4B-Base provided in Appendix B.

**Low-order Plateau- $k$  States: logical branching.** Low-order plateau states typically correspond to semantic or logical branching. In these cases, the model assigns comparable probabilities to a small set of locally plausible tokens, which may include the observed target token and other valid alternatives. Such states indicate that the next-token distribution preserves multiple plausible continuation paths rather than collapsing to one token.

**High-order Plateau- $k$  States: structural ambiguity.** High-order plateau states exhibit qualitatively different behavior. They often arise from structural ambiguity, where the local context does not contain enough information to determine a unique next token. Typical cases include random IDs, dates, timestamps, and URLs. In such positions, the model distributes probability across combinations of digits or characters; in particular, the concentration around  $k = 10$  largely comes from nearly uniform alternatives among the digits 0-9. This suggests that higher-order plateaus capture diffuse structural uncertainty, rather than the semantic branching observed in the low-order regime.

This observation highlights a key limitation of the standard cross-entropy objective used in SFT: it rewards only the observed target token while ignoring the pre-existing entropy structure of the base model’s next-token distribution. For logical branching states, forcing the model toward a single supervised label suppresses other plausible continuation paths and reduces generation diversity. For structural ambiguity states, the next token may be intrinsically underdetermined, such as a random digit or character, so treating one observed token as the only correct target introduces noisy or arbitrary supervision. This provides one possible mechanism for why vanilla SFT can cause catastrophic forgetting and diversity loss: it overwrites the base model’s structured uncertainty instead of preserving useful alternatives.

The boundary between low-order and high-order regimes is not strict. The threshold  $k = 5$  is only a coarse empirical separation, and structural alternatives can also appear in low-order plateau states. Nevertheless, these examples show that the base model already encodes rich distributional knowledge about the local continuation space, often maintaining structured uncertainty over multiple plausible continuations rather than assigning probability mass only to the observed target token.

## 5 Method: Local-Preserving SFT

The multimodal entropy peaks and plateau- $k$  states discussed above show that the pretrained base model encodes rich local preference structures among plausible next-token alternatives. We use  $R = N_2/N_1$  as a diagnostic for identifying near-uniform plateau states, while LP-SFT uses  $N_1$  to choose the adaptive support size because it directly estimates the effective number of plausible alternatives. Based on this observation, we propose **LP-SFT** (**L**ocal-**P**reserving **S**upervised **F**ine-**T**uning), which combines cross-entropy on the supervised token with a local preservation objective over adaptively selected non-target candidates. LP-SFT relies on **target-token removal** to avoid conflict with cross-entropy learning and **local KL normalization** to preserve relative preferences among non-label alternatives.

### 5.1 Adaptive Preservation Set with Target-Token Removal

Given an instruction-response pair with prompt  $\mathbf{x}$  and target sequence  $\mathbf{y} = (y_1, \dots, y_T)$ , we denote the frozen base model distribution and the trainable model distribution at position  $t$  by  $q_t(\cdot) = p_{\theta_0}(\cdot \mid \mathbf{x}, y_{<t})$  and  $p_t(\cdot) = p_{\theta}(\cdot \mid \mathbf{x}, y_{<t})$ , respectively. To determine which local structure should be preserved, LP-SFT first selects a candidate set from the frozen base distribution:

$$S_t = C_{k_t}(q_t), \quad k_t = \min(\lceil N_1(q_t) \rceil, K_{\max}), \quad (13)$$

where  $N_1(q_t)$  is the Shannon effective support size and  $K_{\max}$  is a predefined upper bound. This adaptive support selects a small set of plausible next-token alternatives according to the base model’s local uncertainty.

The first key design of LP-SFT is **target-token removal**. If the preservation objective directly constrained the supervised token  $y_t$ , it could interfere with the cross-entropy loss, which already optimizes  $y_t$ . To decouple target-token learning from local structure preservation, we remove  $y_t$  from  $S_t$  and form the initial non-target support

$$S'_t = S_t \setminus \{y_t\}. \quad (14)$$

If no non-target candidate remains, we skip the preservation term at this position. If only one non-target candidate remains, we add the next most probable non-target token under  $q_t$  to avoid a degenerate one-token preservation set. Specifically, the final preservation set  $\mathcal{A}_t$  is constructed as

$$\mathcal{A}_t = \begin{cases} \emptyset, & \text{if } |S'_t| = 0, \\ S'_t \cup \left\{ \arg \max_{v \notin S_t \cup \{y_t\}} q_t(v) \right\}, & \text{if } |S'_t| = 1, \\ S'_t, & \text{if } |S'_t| \geq 2. \end{cases} \quad (15)$$

When  $|S'_t| = 0$ , the adaptive support contains only the supervised token, leaving no selected non-target alternative to preserve. When  $|S'_t| = 1$ , the added token forms a minimal two-token non-target preservation set. The resulting  $\mathcal{A}_t$  contains only non-label alternatives, over which the locally normalized KL loss is applied in the next subsection.

### 5.2 Local-Preserving Training Objective

Given the final preservation set  $\mathcal{A}_t$ , LP-SFT applies its second key design: **local KL normalization**. When  $\mathcal{A}_t \neq \emptyset$ , we renormalize both the frozen base distribution and the trainable model distribution strictly within this local non-label subset:

$$\hat{q}_t(v) = \frac{q_t(v)}{\sum_{u \in \mathcal{A}_t} q_t(u)}, \quad \hat{p}_t(v) = \frac{p_t(v)}{\sum_{u \in \mathcal{A}_t} p_t(u)}, \quad \forall v \in \mathcal{A}_t. \quad (16)$$

The local preservation loss is then defined as the KL divergence between these two normalized distributions:

$$\mathcal{L}_{\text{LP}}^t = \begin{cases} 0, & \text{if } \mathcal{A}_t = \emptyset, \\ \sum_{v \in \mathcal{A}_t} \hat{q}_t(v) \ln \frac{\hat{q}_t(v)}{\hat{p}_t(v)}, & \text{otherwise.} \end{cases} \quad (17)$$

Since  $\hat{q}_t$  is derived from the frozen base model, it is treated as a fixed target. Minimizing this KL divergence is therefore equivalent, up to a constant independent of  $\theta$ , to minimizing the local cross-entropy  $-\sum_{v \in \mathcal{A}_t} \hat{q}_t(v) \ln \hat{p}_t(v)$ .

Local normalization ensures that the preservation loss focuses on the relative preferences among non-label alternatives rather than their absolute probability mass. This is important because the selected set  $\mathcal{A}_t$  is only

---

**Algorithm 1** LP-SFT Training

---

**Require:** Base model  $\theta_0$ , training dataset  $\mathcal{D}$ , max support  $K_{\max}$ , weight  $\mu$

- 1: // **Stage 1: Offline Base Precomputation**
- 2: **for** each sample  $(\mathbf{x}, \mathbf{y}) \in \mathcal{D}$  **do**
- 3:   Compute  $q_t = p_{\theta_0}(\cdot | \mathbf{x}, y_{<t})$  and cache top- $K_{\max}$  candidate logits and  $k_t$  for all valid  $t$
- 4: **end for**
- 5: // **Stage 2: Local-Preserving Supervised Fine-Tuning**
- 6: **for** each mini-batch from  $\mathcal{D}$  **do**
- 7:    $\mathcal{L} \leftarrow 0$
- 8:   **for** each target position  $t$  **do**
- 9:     Load cached base information and construct  $S_t$  and  $\mathcal{A}_t$  via Eq. (15)
- 10:      $\mathcal{L}_{\text{LP}}^t \leftarrow 0$
- 11:     **if**  $\mathcal{A}_t \neq \emptyset$  **then**
- 12:        $\hat{q}_t, \hat{p}_t \leftarrow \text{Normalize}(q_t|_{\mathcal{A}_t}), \text{Normalize}(p_t|_{\mathcal{A}_t})$
- 13:        $\mathcal{L}_{\text{LP}}^t \leftarrow \sum_{v \in \mathcal{A}_t} \hat{q}_t(v) \ln \frac{\hat{q}_t(v)}{\hat{p}_t(v)}$
- 14:     **end if**
- 15:      $\mathcal{L} \leftarrow \mathcal{L} - \ln p_t(y_t) + \mu \cdot \mathcal{L}_{\text{LP}}^t$
- 16:   **end for**
- 17:   Update parameters  $\theta$  using  $\nabla_{\theta} \mathcal{L}$
- 18: **end for**

---

a truncated local support and may not cover the entire plateau region, especially when the effective support of the base distribution exceeds  $K_{\max}$ . Applying a standard KL divergence to unnormalized probabilities on this truncated set would also constrain the absolute probability mass assigned to  $\mathcal{A}_t$ , implicitly treating probability mass outside the selected set as irrelevant. By normalizing locally, LP-SFT preserves the relative preference structure within  $\mathcal{A}_t$  while leaving its total mass unconstrained. Furthermore, since the target token  $y_t$  is excluded from  $\mathcal{A}_t$ , LP-SFT decouples the learning process: the cross-entropy objective learns the supervised token, while the local KL term preserves the base model’s structural preferences among plausible non-label alternatives.

The final LP-SFT objective is

$$\mathcal{L}_{\text{LP-SFT}}(\theta) = \sum_{t=1}^T [-\ln p_t(y_t) + \mu \mathcal{L}_{\text{LP}}^t], \quad (18)$$

where  $\mu$  controls the preservation strength. Appendix E.1 shows that LP-SFT is relatively insensitive to the choice of  $\mu$ , and Appendix E.2 further indicates that target-token removal and local KL normalization jointly contribute to this stability.

Unlike standard distillation [10, 6, 1], which typically matches a teacher distribution over the full vocabulary at each token position, LP-SFT uses the frozen base model only as a local structural reference over selected non-label alternatives. By applying the base-model constraint within this local normalized support, LP-SFT preserves plateau- $k$  structures while retaining the supervised learning signal, enabling SFT to leverage the local distributional knowledge acquired during pretraining rather than treating the pretrained model merely as an initialization point.

### 5.3 Efficient Implementation

A naive implementation of LP-SFT would require keeping both the frozen base model and the trainable model in memory and running an additional base-model forward pass at each training step. Since the base model  $\theta_0$  is frozen and the training data is fixed, we instead precompute the required base-distribution information offline.

As shown in Algorithm 1, LP-SFT is implemented in two stages. In Stage 1, we perform a single offline pass over the training dataset with the base model and cache the top candidate logits required to construct the adaptive preservation set, together with the adaptive support size  $k_t$ . In Stage 2, fine-tuning proceeds with only the standard forward pass of the trainable model. The local preservation loss  $\mathcal{L}_{\text{LP}}^t$  is computed on the fly using the cached base logits and the current model logits restricted to  $\mathcal{A}_t$ . This decoupling avoids additional base-model forward passes during fine-tuning and adds only a lightweight local KL computation over small candidate sets.

Table 1: **Fine-tuning results on the mixed-domain dataset.** Generation tasks are reported as pass@1/pass@ $k$ ; MMLU is 5-shot accuracy. Avg. is the mean of all displayed scores in each row. Bold numbers indicate the best result among fine-tuned methods, excluding the base model.

Model	Method	Math				Code				GEN.	Avg.
		MATH-500		AIME 23-26		MBPP+		HE+	MMLU		
		pass@1 / pass@16	pass@1 / pass@16	pass@1 / pass@32	pass@1 / pass@32	pass@1 / pass@10	pass@1 / pass@10	pass@1 / pass@10	5-shot Acc.	All	
Qwen3-14B	Base	66.91	87.60	9.22	35.83	69.62	87.88	77.74	93.32	80.51	67.63
	CE	47.27	83.60	6.69	28.33	60.87	82.18	66.22	89.19	76.78	60.13
	DFT	47.75	59.00	4.14	14.17	65.71	69.55	71.04	73.45	75.94	53.42
	EAFT	47.84	83.20	6.88	33.33	60.52	82.58	64.60	86.79	76.80	60.28
	GEM	46.73	85.20	6.07	30.83	51.67	80.41	57.23	87.71	77.08	58.10
	ASFT	52.95	78.20	7.53	29.17	66.90	76.54	69.82	82.75	78.10	60.22
	LP-SFT	<b>59.82</b>	<b>86.80</b>	<b>8.39</b>	<b>35.00</b>	<b>67.94</b>	<b>84.80</b>	<b>73.11</b>	<b>89.71</b>	<b>78.65</b>	<b>64.91</b>

## 6 Experiments

We evaluate **LP-SFT** across multiple model scales and domains, focusing on two questions: (1) whether LP-SFT improves pass@1 accuracy and overall performance over vanilla SFT and recent SFT-enhancement baselines, and (2) whether it mitigates catastrophic forgetting while maintaining sampling-accessible diversity, as reflected by pass@ $k$  performance.

### 6.1 Setup

**Models and datasets.** We evaluate our method across three widely used base large language models spanning different parameter scales: **Qwen3-4B**, **Llama-3.1-8B**, and **Qwen3-14B**. To rigorously test both domain-specific learning and general capability preservation, we select three distinct instruction-tuning datasets: **MagiCoder-OSS-Instruct-75K** for code generation, a 100K subset of **NuminaMath-CoT** for mathematical reasoning, and **UltraFeedback** (61K) for general human alignment.

**Baselines.** We compare LP-SFT with standard supervised fine-tuning using cross-entropy loss (**CE**), Dynamic Fine-Tuning (**DFT**) [22], Entropy-Adaptive Fine-Tuning (**EAFT**) [4], **GEM** [13], and Anchored Supervised Fine-Tuning (**ASFT**) [24]. For LP-SFT, we set the preservation weight to  $\mu = 1$ . When computing the adaptive support size,  $N_1(q_t)$  is estimated from the normalized top-30 base distribution, and we set  $K_{\max} = 10$ .

**Evaluation benchmarks.** We evaluate the fine-tuned models along three capability dimensions: mathematics, coding, and general knowledge reasoning. For **mathematics**, we evaluate on MATH-500 [8] using  $n = 16$  samples, and on a collected set of AIME 2023–2026 problems, consisting of 120 problems, using  $n = 32$  samples. For **coding**, we evaluate on MBPP+ and HumanEval+ (HE+) [14] using  $n = 20$  samples. For **general knowledge**, we report 5-shot accuracy on MMLU [7].

For all generation tasks, we report pass@1 and pass@ $k$ , where  $k = 16$  for MATH-500,  $k = 32$  for AIME, and  $k = 10$  for MBPP+ and HumanEval+. Pass@1 denotes the mean single-sample accuracy over  $n$  i.i.d. samples, while pass@ $k$  estimates the probability of obtaining at least one correct answer within  $k$  sampled outputs [2]. We report both metrics because they capture complementary aspects of model behavior: pass@1 measures single-generation accuracy, while pass@ $k$  reflects sampling-accessible solution diversity. In all result tables, Avg. denotes the mean of all displayed benchmark scores in each row, including pass@1, pass@ $k$ , and MMLU accuracy. More comprehensive training and evaluation details are provided in Appendix C.

### 6.2 Mixed-Domain Fine-Tuning

We first evaluate LP-SFT in a mixed-domain setting, where Qwen3-14B-Base is fine-tuned on a mixture of three datasets covering mathematical reasoning, code generation, and general instruction following. This setting is close to practical SFT scenarios, where diverse training corpora can introduce competing optimization signals and exacerbate catastrophic forgetting. As shown in Table 1, LP-SFT achieves the best results across all displayed metrics among fine-tuned models, covering both pass@1 and pass@ $k$  evaluations.

Compared with CE, LP-SFT substantially improves pass@1 performance across all math and code benchmarks, raising MATH-500 from 47.27 to 59.82, AIME from 6.69 to 8.39, MBPP+ from 60.87 to 67.94, and HE+ from 66.22 to 73.11. It also improves the overall Avg. score from 60.13 to 64.91. Meanwhile, LP-SFT achieves

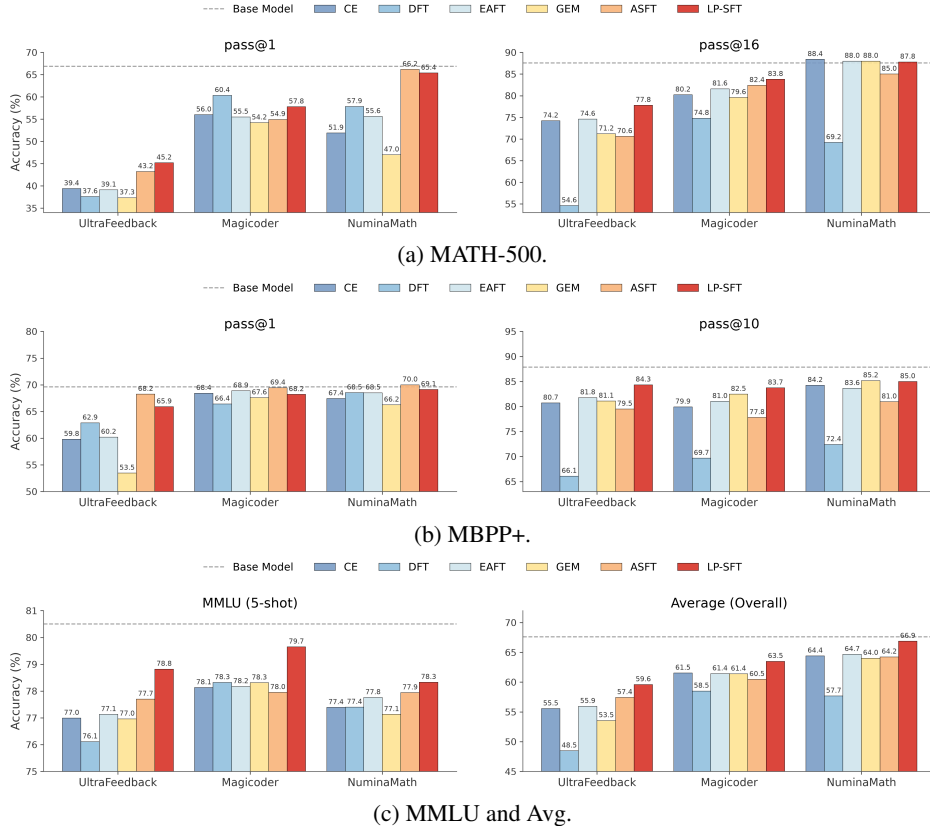


Figure 3: Qwen3-14B fine-tuning results across three training datasets.

the best  $\text{pass}@k$  performance across all displayed sampling-based evaluations, suggesting that it improves single-sample correctness without collapsing sampling-accessible diversity. Compared with the base model, LP-SFT also shows the smallest overall degradation among fine-tuned methods, reducing the Avg. gap from 7.50 points under CE to 2.72 points. These results indicate that preserving the base model’s local distributional structure helps retain pretrained capabilities and mitigate catastrophic forgetting during mixed-domain SFT.

### 6.3 Domain-specific Fine-tuning

We further evaluate LP-SFT under domain-specific fine-tuning on three datasets: UltraFeedback, Magicoder-OSS-Instruct-75K, and NuminaMath-CoT. Figure 3 summarizes the Qwen3-14B results across these datasets, while Table 2 reports detailed UltraFeedback results for Qwen3-4B, Qwen3-14B, and Llama-3.1-8B. Additional results on Magicoder and NuminaMath are provided in Appendix C.2.

Across all combinations of the three backbones and three training datasets, LP-SFT achieves the highest overall average. The gains are most pronounced on UltraFeedback, where general-domain fine-tuning can substantially degrade out-of-domain capabilities such as mathematical reasoning and code generation. LP-SFT mitigates this degradation by preserving the base model’s local distributional structure, improving both overall performance and capability retention. On Magicoder and NuminaMath, LP-SFT also improves the overall average and MMLU accuracy while maintaining competitive task-specific  $\text{pass}@k$  performance. These results suggest that local preservation helps prevent over-collapse toward the supervised target and better maintains sampling-accessible knowledge during domain-specific fine-tuning.

**Comparison with baselines.** Figure 3 highlights different trade-offs between accuracy and diversity among the baselines. DFT improves  $\text{pass}@1$  in some cases, but often leads to a large drop in  $\text{pass}@k$ , suggesting reduced sampling diversity. ASFT partially alleviates this issue by adding a base-model anchoring term, but it still does not fully recover  $\text{pass}@k$  performance. In contrast, GEM better preserves  $\text{pass}@k$  but provides weaker  $\text{pass}@1$  gains. LP-SFT achieves the strongest overall trade-off by improving  $\text{pass}@1$  while maintaining competitive or

Table 2: **Fine-tuning results on UltraFeedback.** Generation tasks are reported as pass@1/pass@ $k$ ; MMLU is 5-shot accuracy. Avg. is the mean of all displayed scores in each row.

Model	Method	Math				Code				GEN.	Avg.
		MATH-500		AIME 23-26		MBPP+		HE+	MMLU		
		pass@1 / pass@16	pass@1 / pass@16	pass@1 / pass@32	pass@1 / pass@32	pass@1 / pass@10	pass@1 / pass@10	pass@1 / pass@10	5-shot Acc.	All	
Qwen3-4B	CE	35.60	72.60	1.80	15.00	46.28	66.25	58.11	84.57	68.90	49.90
	DFT	34.31	52.40	0.62	4.17	<b>54.22</b>	58.95	60.52	64.21	66.82	44.02
	EAFT	35.88	73.00	1.82	15.00	48.94	71.13	59.76	84.38	69.08	51.00
	GEM	33.26	72.60	1.35	15.00	43.96	69.54	54.48	85.34	68.99	49.39
	ASFT	40.71	70.00	1.54	13.33	52.60	65.22	63.20	78.63	69.54	50.53
	LP-SFT	<b>42.79</b>	<b>76.80</b>	<b>2.47</b>	<b>20.83</b>	51.60	<b>76.49</b>	<b>64.42</b>	<b>86.91</b>	<b>70.32</b>	<b>54.74</b>
Qwen3-14B	CE	39.39	74.20	2.16	15.83	59.81	80.71	62.96	87.85	76.99	55.54
	DFT	37.59	54.60	1.38	8.33	62.87	66.08	61.92	67.37	76.11	48.47
	EAFT	39.10	74.60	1.98	17.50	60.21	81.77	63.38	87.78	77.13	55.94
	GEM	37.34	71.20	1.95	15.83	53.47	81.09	57.07	87.06	76.96	53.55
	ASFT	43.23	70.60	<b>2.92</b>	<b>21.67</b>	<b>68.25</b>	79.50	71.25	81.79	77.70	57.43
	LP-SFT	<b>45.19</b>	<b>77.80</b>	2.76	19.17	65.90	<b>84.34</b>	<b>72.13</b>	<b>90.16</b>	<b>78.82</b>	<b>59.59</b>
Llama3.1-8B	CE	<b>9.95</b>	<b>42.60</b>	<b>0.26</b>	<b>6.67</b>	31.61	51.04	32.32	59.12	61.11	32.74
	DFT	4.76	14.60	<b>0.26</b>	5.83	26.19	32.55	25.27	32.18	55.11	21.86
	EAFT	8.35	40.00	0.18	5.83	27.08	49.91	<b>34.15</b>	59.50	61.14	31.79
	GEM	8.19	41.40	0.18	5.00	30.34	54.33	32.44	<b>62.84</b>	61.00	32.86
	ASFT	7.90	33.40	0.05	1.67	35.70	55.49	30.50	51.07	60.58	30.71
	LP-SFT	8.48	40.00	0.10	3.33	<b>37.94</b>	<b>63.95</b>	30.18	59.60	<b>62.48</b>	<b>34.01</b>

improved pass@ $k$  performance, indicating that local preservation helps retain sampling-accessible diversity without sacrificing single-sample accuracy.

Table 2 further shows that LP-SFT is particularly effective for the stronger Qwen3 backbones, especially on mathematical benchmarks. For Llama-3.1-8B, however, CE remains stronger on several math metrics. This suggests that the benefit of local preservation may depend on the quality of the pretrained distribution: stronger base models provide more reliable local structure to preserve, while weaker base models may benefit more from direct target fitting through CE on some tasks.

**Additional Analyses.** We further conduct ablation studies on the preservation weight  $\mu$ , preservation-set construction, KL scope, and support schedule. The results show that target-token removal and local KL normalization are both important for stable preservation, and that local preservation performs comparably or slightly better than full-vocabulary KL while avoiding unnecessary global constraints. We also compare the default  $N_1$ -adaptive schedule with a fixed top-10 schedule, showing that the choice of  $k_t$  can affect performance across backbone models. Finally, training-cost comparisons show that LP-SFT adds only modest overhead over CE and is substantially more efficient than full-vocabulary anchoring methods such as ASFT. Detailed ablation and efficiency results are provided in Appendix E.

## 7 Conclusion

We presented LP-SFT, a local-preserving supervised fine-tuning objective that preserves the local preference structure of the pretrained model while learning from supervised target tokens. Motivated by the multimodal entropy structure observed in base-model distributions, LP-SFT preserves adaptive non-label supports to reduce unnecessary distributional distortion. Across mixed-domain and single-domain fine-tuning experiments, LP-SFT improves overall performance over vanilla SFT and recent SFT-enhancement baselines, achieving the strongest aggregate performance across pass@1 and pass@ $k$  metrics while maintaining competitive sampling-accessible diversity. These results suggest that local preservation is an effective way to mitigate catastrophic forgetting during supervised fine-tuning.

## References

- [1] Rishabh Agarwal, Nino Vieillard, Yongchao Zhou, Piotr Stanczyk, Sabela Ramos Garea, Matthieu Geist, and Olivier Bachem. On-policy distillation of language models: Learning from self-generated mistakes. In *International Conference on Learning Representations*, volume 2024, pages 21246–21263, 2024.

- [2] Mark Chen, Jerry Tworek, Heewoo Jun, Qiming Yuan, Henrique Ponde De Oliveira Pinto, Jared Kaplan, Harri Edwards, Yuri Burda, Nicholas Joseph, Greg Brockman, et al. Evaluating large language models trained on code. *arXiv preprint arXiv:2107.03374*, 2021.
- [3] Ganqu Cui, Lifan Yuan, Ning Ding, Guanming Yao, Bingxiang He, Wei Zhu, Yuan Ni, Guotong Xie, Ruobing Xie, Yankai Lin, et al. Ultrafeedback: Boosting language models with scaled ai feedback. *arXiv preprint arXiv:2310.01377*, 2023.
- [4] Muxi Diao, Lele Yang, Wuxuan Gong, Yutong Zhang, Zhonghao Yan, Yufei Han, Kongming Liang, Weiran Xu, and Zhanyu Ma. Entropy-adaptive fine-tuning: Resolving confident conflicts to mitigate forgetting. *arXiv preprint arXiv:2601.02151*, 2026.
- [5] Aaron Grattafiori, Abhimanyu Dubey, Abhinav Jauhri, Abhinav Pandey, Abhishek Kadian, Ahmad Al-Dahle, Aiesha Letman, Akhil Mathur, Alan Schelten, Alex Vaughan, et al. The llama 3 herd of models. *arXiv preprint arXiv:2407.21783*, 2024.
- [6] Yuxian Gu, Li Dong, Furu Wei, and Minlie Huang. Minillm: Knowledge distillation of large language models. In *International Conference on Learning Representations*, volume 2024, pages 32694–32717, 2024.
- [7] Dan Hendrycks, Collin Burns, Steven Basart, Andy Zou, Mantas Mazeika, Dawn Song, and Jacob Steinhardt. Measuring massive multitask language understanding. *arXiv preprint arXiv:2009.03300*, 2020.
- [8] Dan Hendrycks, Collin Burns, Saurav Kadavath, Akul Arora, Steven Basart, Eric Tang, Dawn Song, and Jacob Steinhardt. Measuring mathematical problem solving with the math dataset. *arXiv preprint arXiv:2103.03874*, 2021.
- [9] Mark O Hill. Diversity and evenness: a unifying notation and its consequences. *Ecology*, 54(2):427–432, 1973.
- [10] Geoffrey Hinton, Oriol Vinyals, and Jeff Dean. Distilling the knowledge in a neural network. *arXiv preprint arXiv:1503.02531*, 2015.
- [11] Lou Jost. Entropy and diversity. *Oikos*, 113(2):363–375, 2006.
- [12] Jia Li, Edward Beeching, Lewis Tunstall, Ben Lipkin, Roman Soletskyi, Shengyi Huang, Kashif Rasul, Longhui Yu, Albert Q Jiang, Ziju Shen, et al. Numinamath: The largest public dataset in ai4maths with 860k pairs of competition math problems and solutions. *Hugging Face repository*, 13(9):9, 2024.
- [13] Ziniu Li, Congliang Chen, Tian Xu, Zeyu Qin, Jiancong Xiao, Zhi-Quan Luo, and Ruoyu Sun. Preserving diversity in supervised fine-tuning of large language models. In *International Conference on Learning Representations*, volume 2025, pages 66127–66154, 2025.
- [14] Jiawei Liu, Chunqiu Steven Xia, Yuyao Wang, and Lingming Zhang. Is your code generated by chatgpt really correct? rigorous evaluation of large language models for code generation. *Advances in neural information processing systems*, 36:21558–21572, 2023.
- [15] Yun Luo, Zhen Yang, Fandong Meng, Yafu Li, Jie Zhou, and Yue Zhang. An empirical study of catastrophic forgetting in large language models during continual fine-tuning. *IEEE Transactions on Audio, Speech and Language Processing*, 2025.
- [16] Long Ouyang, Jeffrey Wu, Xu Jiang, Diogo Almeida, Carroll Wainwright, Pamela Mishkin, Chong Zhang, Sandhini Agarwal, Katarina Slama, Alex Ray, et al. Training language models to follow instructions with human feedback. *Advances in neural information processing systems*, 35:27730–27744, 2022.
- [17] Shenzhi Wang, Le Yu, Chang Gao, Chujie Zheng, Shixuan Liu, Rui Lu, Kai Dang, Xiong-Hui Chen, Jianxin Yang, Zhenru Zhang, et al. Beyond the 80/20 rule: High-entropy minority tokens drive effective reinforcement learning for llm reasoning. *Advances in Neural Information Processing Systems*, 38:115452–115486, 2026.
- [18] Yizhong Wang, Yeganeh Kordi, Swaroop Mishra, Alisa Liu, Noah A Smith, Daniel Khoshabi, and Hannaneh Hajishirzi. Self-instruct: Aligning language models with self-generated instructions. In *Proceedings of the 61st annual meeting of the association for computational linguistics (volume 1: long papers)*, pages 13484–13508, 2023.
- [19] Yueyang Wang, Jiawei Fu, Baolong Bi, Xili Wang, and Xiaoqing Liu. He-snr: Uncovering latent logic via entropy for guiding mid-training on swe-bench. *arXiv preprint arXiv:2601.20255*, 2026.
- [20] Yuxiang Wei, Zhe Wang, Jiawei Liu, Yifeng Ding, and Lingming Zhang. Magicoder: Empowering code generation with oss-instruct. *arXiv preprint arXiv:2312.02120*, 2023.

- [21] Sean Welleck, Ilya Kulikov, Stephen Roller, Emily Dinan, Kyunghyun Cho, and Jason Weston. Neural text generation with unlikelihood training. *arXiv preprint arXiv:1908.04319*, 2019.
- [22] Yongliang Wu, Yizhou Zhou, Zhou Ziheng, Yingzhe Peng, Xinyu Ye, Xinting Hu, Wenbo Zhu, Lu Qi, Ming-Hsuan Yang, and Xu Yang. On the generalization of sft: A reinforcement learning perspective with reward rectification. *arXiv preprint arXiv:2508.05629*, 2025.
- [23] An Yang, Anfeng Li, Baosong Yang, Beichen Zhang, Binyuan Hui, Bo Zheng, Bowen Yu, Chang Gao, Chengen Huang, Chenxu Lv, et al. Qwen3 technical report. *arXiv preprint arXiv:2505.09388*, 2025.
- [24] He Zhu, Junyou Su, Peng Lai, Ren Ma, Wenjia Zhang, Linyi Yang, and Guanhua Chen. Anchored supervised fine-tuning. *arXiv preprint arXiv:2509.23753*, 2025.

## A Derivation of the Finite-top- $K$ Lower Envelope

We derive the finite-top- $K$  lower-envelope branch of  $R$  for a given Shannon effective support size  $N_1$ . Let  $\hat{p} = (\hat{p}_1, \dots, \hat{p}_K)$  denote the normalized top- $K$  next-token distribution. For a fixed  $N_1$ , minimizing  $R$  is equivalent to minimizing  $N_2$ , or equivalently maximizing the collision probability  $\sum_{i=1}^K \hat{p}_i^2$ , under a fixed Shannon entropy constraint:

$$\begin{aligned} \max_{\hat{p}} \quad & \sum_{i=1}^K \hat{p}_i^2 \\ \text{s.t.} \quad & \begin{cases} \sum_{i=1}^K \hat{p}_i = 1, \\ -\sum_{i=1}^K \hat{p}_i \ln \hat{p}_i = \ln N_1, \\ \hat{p}_i \geq 0, \quad i = 1, \dots, K. \end{cases} \end{aligned} \quad (19)$$

The Lagrangian of this constrained optimization problem is

$$\mathcal{L} = \sum_{i=1}^K \hat{p}_i^2 - \lambda \left( \sum_{i=1}^K \hat{p}_i - 1 \right) - \mu \left( -\sum_{i=1}^K \hat{p}_i \ln \hat{p}_i - \ln N_1 \right). \quad (20)$$

For any positive component  $\hat{p}_i > 0$ , the stationarity condition gives

$$\frac{\partial \mathcal{L}}{\partial \hat{p}_i} = 2\hat{p}_i - \lambda + \mu(\ln \hat{p}_i + 1) = 0, \quad (21)$$

or equivalently

$$2\hat{p}_i + \mu \ln \hat{p}_i = C, \quad (22)$$

where  $C = \lambda - \mu$  is a constant independent of  $i$ . Since the scalar equation  $2x + \mu \ln x = C$  has at most two positive solutions, any interior stationary extremum has at most two distinct positive probability values. Boundary extrema are covered by allowing some probabilities to be zero.

Therefore, the general two-level extremal family can be written as

$$\hat{p}^\dagger(j, m, a, b) = \left( \underbrace{a, \dots, a}_j, \underbrace{b, \dots, b}_{m-j}, 0, \dots, 0 \right), \quad (23)$$

where

$$a > b \geq 0, \quad 1 \leq j \leq m-1, \quad 2 \leq m \leq K. \quad (24)$$

The values  $(a, b)$  are determined by the normalization and entropy constraints

$$ja + (m-j)b = 1, \quad -ja \ln a - (m-j)b \ln b = \ln N_1. \quad (25)$$

Among these two-level candidates, the lower-envelope branch observed in the  $(N_1, R)$  plane is attained by the most asymmetric case, where the larger probability value appears once. Intuitively, concentrating the high-probability mass on a single coordinate increases the collision probability, while the remaining mass forms

a uniform residual tail. We verified this reduction by enumerating all feasible  $(j, m)$  in the finite range used in our analysis, with  $m \in \{2, \dots, 30\}$  and  $N_1 \in (1, m]$ , and the lower branch is attained by  $j = 1$ .

Thus, the relevant extremal family reduces to the one-dominant / uniform-tail form

$$\hat{p}^*(q, m) = \left( q, \underbrace{\frac{1-q}{m-1}, \dots, \frac{1-q}{m-1}}_{m-1 \text{ entries}}, 0, \dots, 0 \right), \quad q \in [1/m, 1], \quad m \in \{2, \dots, K\}. \quad (26)$$

For this family, the Shannon entropy is

$$H_1(q, m) = -q \ln q - (1-q) \ln \frac{1-q}{m-1}, \quad (27)$$

and the collision probability is

$$\sum_{i=1}^K \hat{p}_i^2 = q^2 + \frac{(1-q)^2}{m-1}. \quad (28)$$

The finite-top- $K$  lower-envelope branch can then be written as

$$R_{\min}(N_1; K) = \min_{2 \leq m \leq K, q \in [1/m, 1]} \frac{1}{N_1 \left[ q^2 + \frac{(1-q)^2}{m-1} \right]} \quad \text{s.t.} \quad H_1(q, m) = \ln N_1. \quad (29)$$

Infeasible values of  $m$  are automatically excluded by the entropy constraint  $H_1(q, m) = \ln N_1$ . In our experiments,  $K = 30$ , since both  $N_1$  and  $N_2$  are computed from the normalized top- $K$  distribution with  $K = 30$ .

## B Representative Plateau Examples

We provide representative token-level examples for different plateau orders. Each example shows a truncated context window around the ground-truth target token, with the target highlighted, together with the corresponding prediction distribution. For  $k \leq 10$ , we show the top-10 candidates; for  $k > 10$ , we show the top-20 candidates.

**Instance 1:**  $k = 2$    **Target Token:** of    $N_1: 2.000$     $R: 1.0000$

```

Context Window (Truncated)
1 To solve for \(\ x \), we first combine like terms:
2
3 \[\ \frac{7}{2}x = 14 \]
4
5 Now, we multiply both sides of the equation by \(\ \frac{2}{7} \) to
  isolate \(\ x \):
6
7 \[\ x = 14 \times \frac{2}{7} \]

```

Table 3: Top-10 Prediction Distribution for Instance 1 ( $k = 2$ ).

Rank	Token	Prob.	Rank	Token	Prob.
1	of	0.500	6	by	0.000
2	by	0.500	7	By	0.000
3	with	0.000	8	of	0.000
4	cua	0.000	9	the	0.000
5	to	0.000	10	Thai-of	0.000

**Instance 2:**  $k = 3$  **Target Token:** divide  $N_1$ : 3.000  $R$ : 0.9999

**Context Window (Truncated)**

```

1 7000(1 + r/1)^(1*2)
2 19828.80 = 17000(1 + r)^2
3
4 Now, divide both sides by 17000:
5
6 19828.80 / 17000 = (1 + r)^2

```

Table 4: Top-10 Prediction Distribution for Instance 2 ( $k = 3$ ).

Rank	Token	Prob.	Rank	Token	Prob.
1	divide	0.333	6	dividing	0.000
2	let	0.333	7	simplify	0.000
3	we	0.333	8	to	0.000
4	solve	0.000	9	divided	0.000
5	divide	0.000	10	square	0.000

**Instance 3:**  $k = 4$  **Target Token:** +  $N_1$ : 4.029  $R$ : 0.9945

**Context Window (Truncated)**

```

1 + 1 - \frac{3}{ax} \\
2 &= \frac{2a^2x^2 + ax - 3}{ax} \\
3 &= \frac{(2ax + 3)(ax - 1)}{ax}.
4 \end{aligned}
5 \]
6
7 For  $(x=1)$  to be a critical point,  $(f'(1)=0)$ . Plugging in  $($ 
```

Table 5: Top-10 Prediction Distribution for Instance 3 ( $k = 4$ ).

Rank	Token	Prob.	Rank	Token	Prob.
1	␣-	0.250	6	^	0.000
2	-	0.250	7	+␣	0.000
3	+	0.250	8	-␣	0.000
4	␣+	0.250	9	+a	0.000
5	)^	0.000	10	-	0.000

**Instance 4:**  $k = 5$  **Target Token:** 7  $N_1$ : 5.277  $R$ : 0.9647

**Context Window (Truncated)**

```

1 Keim, SC (2004) "Risk perceptions and safety compliance of workers employed
  in agriculture, forestry, and fishing." Journal of Safety Research
  35(2), 237-244.

```

Table 6: Top-10 Prediction Distribution for Instance 4 ( $k = 5$ ).

Rank	Token	Prob.	Rank	Token	Prob.
1	5	0.198	6	-	0.003
2	3	0.198	7	4	0.001
3	7	0.198	8	6	0.001
4	1	0.198	9	0	0.001
5	9	0.198	10	2	0.001

**Instance 5:**  $k = 6$  **Target Token:** 4  $N_1$ : 6.021  $R$ : 0.9972

**Context Window (Truncated)**

A. G., & Tuuli, M. G. (2016). Maternal marijuana use and adverse neonatal outcomes. *Obstetrics & Gynecology*, 128(4), 713-723.

Table 7: Top-10 Prediction Distribution for Instance 5 ( $k = 6$ ).

Rank	Token	Prob.	Rank	Token	Prob.
1	2	0.167	6	3	0.167
2	1	0.167	7	7	0.000
3	6	0.167	8	9	0.000
4	5	0.167	9	8	0.000
5	4	0.167	10	0	0.000

**Instance 6:**  $k = 7$  **Target Token:** 3  $N_1$ : 7.073  $R$ : 0.9722

**Context Window (Truncated)**

According to a 2021 Gallup poll, 54% of Americans support the death penalty for murder, while 43% oppose it.

Table 8: Top-10 Prediction Distribution for Instance 6 ( $k = 7$ ).

Rank	Token	Prob.	Rank	Token	Prob.
1	2	0.167	6	4	0.131
2	1	0.167	7	5	0.102
3	6	0.167	8	7	0.003
4	3	0.131	9	8	0.001
5	0	0.131	10	9	0.000

**Instance 7:**  $k = 8$  **Target Token:** 4  $N_1$ : 8.285  $R$ : 0.9733

**Context Window (Truncated)**

'Authorization' => 'Basic NTZmZGJmN2EtODUxYy00M2RiLTk4YWUtYTBhZmEzYzFjZGRi',

Table 9: Top-10 Prediction Distribution for Instance 7 ( $k = 8$ ).

Rank	Token	Prob.	Rank	Token	Prob.
1	x	0.159	6	2	0.110
2	1	0.125	7	4	0.110
3	z	0.125	8	5	0.110
4	0	0.125	9	zM	0.011
5	3	0.125	10	...	0.000

**Instance 8:**  $k = 9$  **Target Token:** 6  $N_1$ : 9.033  $R$ : 0.9974

**Context Window (Truncated)**

1 Link: <https://www.inc.com/guides/2010/06/8-entrepreneurial-myths.html>

Table 10: Top-10 Prediction Distribution for Instance 8 ( $k = 9$ ).

Rank	Token	Prob.	Rank	Token	Prob.
1	4	0.111	6	7	0.111
2	3	0.111	7	5	0.111
3	1	0.111	8	2	0.111
4	6	0.111	9	9	0.111
5	8	0.111	10	0	0.000

**Instance 9:**  $k = 10$  **Target Token:** 0  $N_1$ : 10.001  $R$ : 0.9999

**Context Window (Truncated)**

1 | Household Type | Number of Households | Percentage |  
 2 | --- | --- | --- |  
 3 | Single-person households | 1,598,806 | 54.0% |

Table 11: Top-10 Prediction Distribution for Instance 9 ( $k = 10$ ).

Rank	Token	Prob.	Rank	Token	Prob.
1	3	0.100	6	6	0.100
2	2	0.100	7	0	0.100
3	4	0.100	8	1	0.100
4	5	0.100	9	9	0.100
5	7	0.100	10	8	0.100

**Instance 10:**  $k = 12$  **Target Token:** 9  $N_1$ : 11.998  $R$ : 0.9981

**Context Window (Truncated)**

1 i.pining.com/originals/54/ba/82/54ba8283ca60486b3acd27528d7faec9.jpg) |  
 Set up a dedicated space with simple building blocks ...

Table 12: Top-20 Prediction Distribution for Instance 10 ( $k = 12$ ).

Rank	Token	Prob.	Rank	Token	Prob.
1	b	0.092	11	2	0.082
2	f	0.092	12	3	0.082
3	7	0.082	13	d	0.000
4	6	0.082	14	<eot>	0.000
5	1	0.082	15	ac	0.000
6	0	0.082	16	g	0.000
7	4	0.082	17	ab	0.000
8	5	0.082	18	fa	0.000
9	8	0.082	19	=	0.000
10	9	0.082	20	ad	0.000

**Instance 11:**  $k = 15$    **Target Token:** a    $N_1: 14.966$     $R: 0.9969$

```

Context Window (Truncated)
| STEM Corner | [Image](https://i.pining.com/originals/54/ba8283ca60486b3acd27528d7faec9.jpg) | Set up a dedicated space ...

```

Table 13: Top-20 Prediction Distribution for Instance 11 ( $k = 15$ ).

Rank	Token	Prob.	Rank	Token	Prob.
1	4	0.070	11	8	0.062
2	5	0.070	12	3	0.062
3	1	0.070	13	7	0.062
4	9	0.070	14	6	0.062
5	b	0.070	15	f	0.055
6	a	0.070	16	e	0.000
7	d	0.070	17	ad	0.000
8	0	0.070	18	ab	0.000
9	c	0.070	19	fa	0.000
10	2	0.062	20	da	0.000

## C Training and Evaluation Details

### C.1 Training Details

All models are fine-tuned using the HuggingFace Transformers library with DeepSpeed ZeRO Stage-2 for memory-efficient distributed training. We use the AdamW optimizer with a learning rate of  $2 \times 10^{-5}$ , a cosine learning-rate schedule, and a warmup ratio of 0.03. The weight decay is set to 0.0, and we use  $\beta_2 = 0.95$  for AdamW. All models are trained for 3 epochs in bfloat16 precision with gradient checkpointing enabled. The maximum sequence length is set to 2048 tokens, and the random seed is fixed to 1234 for reproducibility. We target an effective batch size of 128 across all experiments. All experiments are conducted on nodes equipped with  $8 \times$  NVIDIA A100 (80GB) GPUs.

**Baseline.** For the GEM baseline, we set the temperature parameter to  $\beta = 0.7$ . For EAFT, we use  $\alpha = 1.0$  and top- $k = 20$ . For ASFT, we set the weight of the full-vocabulary KL loss to 0.05.

### C.2 Evaluation Details

**General evaluation protocol.** All SFT models are evaluated using the chat prompt template of their respective model family (ChatML for Qwen3 and the Llama-3.1 instruct format for Llama-3.1-8B), with thinking mode disabled for Qwen3 models (`enable_thinking=False`) to ensure a fair comparison under standard non-thinking generation. For base models, we use the corresponding base-model prompting format when evaluating generation tasks, without applying instruction-tuned chat-specific behavior. MMLU is the sole exception, where

Table 14: **Base model reference scores.** Performance of the pretrained base models on the same evaluation suite used in our SFT experiments without any fine-tuning. Generation tasks are reported as pass@1/pass@k; MMLU is 5-shot accuracy. Avg. is the mean of all displayed scores in each row.

Model	Math				Code				GEN.	Avg.
	MATH-500		AIME 23-26		MBPP+		HE+		MMLU	
	pass@1 / pass@16	pass@1 / pass@32	pass@1 / pass@10	pass@1 / pass@10	pass@1 / pass@10	pass@1 / pass@10	5-shot Acc.	All		
Qwen3-4B-Base	33.04	79.60	7.53	32.50	59.95	82.29	67.74	90.83	73.10	58.51
Qwen3-14B-Base	66.91	87.60	9.22	35.83	69.62	87.88	77.74	93.32	80.51	67.63
Llama-3.1-8B	8.14	41.00	0.05	1.67	42.74	72.12	27.41	66.21	65.28	36.07

all models are evaluated with the base non-chat prompt format to avoid formatting artifacts in log-likelihood scoring. We employ vLLM as the inference backend across all benchmarks to accelerate evaluation.

**Mathematical reasoning.** For MATH-500, we use temperature  $T = 0.6$ ,  $n = 16$  samples,  $\text{top}_p = 1.0$ , and a maximum generation length of 4096 tokens. We report pass@1 and pass@16. For AIME, we use temperature  $T = 0.6$ ,  $n = 32$  samples,  $\text{top}_p = 1.0$ , a maximum generation length of 8192 tokens, and  $\text{max\_model\_len}=12288$ . The AIME evaluation is conducted on 120 problems collected from AIME competitions from 2023 to 2026, and we report pass@1 and pass@32.

**Code generation.** HumanEval+ and MBPP+ are evaluated using the EvalPlus framework. We use temperature  $T = 0.8$  and generate  $n = 20$  samples per problem. We report pass@1 and pass@10 for both the base tests and the plus tests with additional hidden test cases.

**General knowledge and reasoning.** For general knowledge and reasoning, we evaluate MMLU in the 5-shot setting using log-likelihood scoring with the lm-evaluation-harness framework.

## D Additional Results

This section reports additional fine-tuning results on individual training datasets, together with the reference scores of the corresponding pretrained base models. All evaluations follow the same protocol as in the main text. For generation tasks, we report pass@1 and pass@k; MMLU is evaluated with 5-shot accuracy. In each table, Avg. denotes the mean of all displayed scores in the corresponding row.

Table 15: **Fine-tuning results on Magicode-OSS-Instruct-75K.** Generation tasks are reported as pass@1/pass@k; MMLU is 5-shot accuracy. Avg. is the mean of all displayed scores in each row.

Model	Method	Math				Code				GEN.	Avg.
		MATH-500		AIME 23-26		MBPP+		HE+		MMLU	
		pass@1 / pass@16	pass@1 / pass@32	pass@1 / pass@10	pass@1 / pass@10	pass@1 / pass@10	pass@1 / pass@10	5-shot Acc.	All		
Qwen3-4B	CE	55.36	80.60	5.78	27.50	60.42	72.40	<b>67.41</b>	80.56	68.93	57.66
	DFT	<b>56.77</b>	71.60	5.83	21.67	58.99	62.68	64.15	66.12	<b>69.63</b>	53.05
	EAFT	54.64	80.60	5.94	28.33	61.20	73.55	66.98	84.76	68.69	58.30
	GEM	53.87	80.00	5.34	29.17	60.19	76.21	66.22	84.95	68.72	58.30
	ASFT	55.05	79.20	2.89	18.33	<b>61.60</b>	71.12	64.88	75.17	69.54	55.31
	LP-SFT	54.86	<b>82.60</b>	<b>6.82</b>	<b>35.83</b>	60.19	<b>78.93</b>	66.04	<b>86.52</b>	69.55	<b>60.15</b>
Qwen3-14B	CE	55.99	80.20	5.36	24.17	68.43	79.92	<b>75.37</b>	86.17	78.13	61.53
	DFT	<b>60.35</b>	74.80	<b>7.19</b>	25.00	66.42	69.67	70.70	74.15	78.32	58.51
	EAFT	55.49	81.60	4.51	22.50	68.88	81.03	73.54	87.05	78.17	61.42
	GEM	54.20	79.60	4.71	22.50	67.59	82.46	73.35	<b>89.74</b>	78.31	61.38
	ASFT	54.94	82.40	6.17	25.00	<b>69.44</b>	77.81	70.06	80.46	77.95	60.47
	LP-SFT	57.79	<b>83.80</b>	5.68	<b>30.83</b>	68.20	<b>83.73</b>	73.32	88.53	<b>79.65</b>	<b>63.50</b>
Llama3.1-8B	CE	6.48	30.80	0.05	1.67	<b>46.92</b>	62.31	<b>41.92</b>	62.05	61.69	34.88
	DFT	5.55	14.60	0.00	0.00	30.70	35.98	22.74	25.81	59.44	21.65
	EAFT	6.34	31.20	0.03	0.83	42.01	60.73	36.83	61.54	60.60	33.35
	GEM	5.65	31.40	<b>0.10</b>	<b>3.33</b>	46.49	65.39	39.41	<b>64.10</b>	61.27	35.24
	ASFT	6.20	25.80	0.05	1.67	43.36	57.21	31.83	48.05	60.77	30.55
	LP-SFT	<b>7.31</b>	<b>34.40</b>	0.05	1.67	46.52	<b>66.91</b>	38.63	61.79	<b>62.11</b>	<b>35.49</b>

Table 16: **Fine-tuning results on NuminaMath-CoT.** Generation tasks are reported as pass@1/pass@k; MMLU is 5-shot accuracy. Avg. is the mean of all displayed scores in each row.

Model	Method	Math				Code				GEN.	Avg.
		MATH-500		AIME 23-26		MBPP+		HE+	MMLU		
		pass@1 / pass@16	pass@1 / pass@32	pass@1 / pass@10	pass@1 / pass@10	pass@1 / pass@10	5-shot Acc.	All			
Qwen3-4B	CE	59.54	85.60	4.61	25.00	57.01	77.17	66.95	87.65	69.69	59.25
	DFT	54.74	69.40	5.26	13.33	<b>60.74</b>	65.91	61.49	67.88	69.09	51.98
	EAFT	59.84	85.00	4.87	29.17	56.12	76.00	<b>68.93</b>	88.84	68.99	59.75
	GEM	55.75	86.00	4.95	<b>30.00</b>	54.15	77.53	66.31	<b>89.25</b>	69.15	59.23
	ASFT	<b>60.94</b>	84.20	6.98	28.33	57.51	72.70	67.01	84.31	69.41	59.04
	LP-SFT	60.00	<b>86.20</b>	<b>7.29</b>	29.17	57.96	<b>78.81</b>	68.35	89.05	<b>69.95</b>	<b>60.75</b>
Qwen3-14B	CE	51.89	<b>88.40</b>	8.98	33.33	67.42	84.24	76.37	91.70	77.39	64.41
	DFT	57.85	69.20	6.28	15.83	68.52	72.41	73.38	78.20	77.40	57.67
	EAFT	55.61	88.00	8.70	31.67	68.51	83.63	<b>76.71</b>	91.40	77.76	64.67
	GEM	46.99	88.00	8.12	35.00	66.24	<b>85.17</b>	76.65	<b>92.93</b>	77.13	64.03
	ASFT	<b>66.20</b>	85.00	8.85	27.50	<b>70.00</b>	80.95	75.40	86.36	77.94	64.24
	LP-SFT	65.38	87.80	<b>10.00</b>	<b>37.50</b>	69.13	84.98	75.95	92.85	<b>78.33</b>	<b>66.88</b>
Llama3.1-8B	CE	<b>31.62</b>	69.00	0.70	10.00	30.09	60.80	24.09	58.85	61.60	38.53
	DFT	14.22	27.00	0.16	3.33	21.75	32.17	8.41	15.89	55.14	19.79
	EAFT	29.35	66.60	<b>0.73</b>	<b>14.17</b>	31.75	63.47	22.96	57.43	60.00	38.50
	GEM	27.14	<b>69.80</b>	0.65	12.50	25.50	59.78	20.40	52.43	60.55	36.53
	ASFT	26.10	59.20	0.52	7.50	31.87	57.37	21.90	47.50	60.22	34.69
	LP-SFT	27.44	66.40	0.42	6.67	<b>35.81</b>	<b>66.75</b>	<b>27.77</b>	<b>60.76</b>	<b>61.94</b>	<b>39.33</b>

## E Additional Ablation and Efficiency Results

This section provides additional analyses of LP-SFT, including sensitivity to the preservation weight  $\mu$ , ablations on the preservation-set construction and support schedule, and training efficiency comparisons.

### E.1 Sensitivity to the Preservation Weight

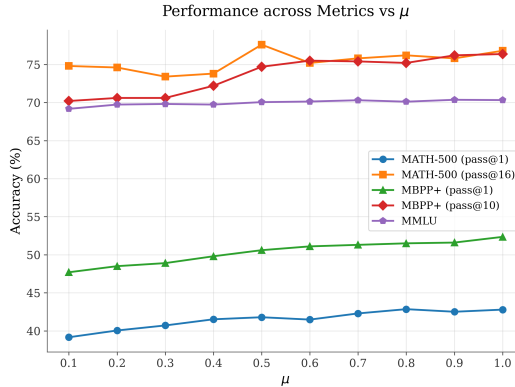


Figure 4: **Sensitivity to the preservation weight  $\mu$ .** Results are obtained with Qwen3-4B fine-tuned on UltraFeedback and evaluated on MATH-500, MBPP+, and MMLU. Performance varies only slightly across  $\mu \in [0.1, 1.0]$ , suggesting that LP-SFT is relatively insensitive to the choice of  $\mu$ .

Figure 4 studies the effect of the preservation weight  $\mu$ . Across the tested range, LP-SFT exhibits only mild performance variation on MATH-500, MBPP+, and MMLU. This suggests that the proposed local preservation objective is stable and does not require careful tuning of  $\mu$ . We therefore use  $\mu = 1$  as the default setting in our main experiments.

### E.2 Ablation on Preservation Set and Support Schedule

Table 17 analyzes how different preservation-set design choices affect LP-SFT on Qwen3-4B-Base trained with UltraFeedback. We consider three factors: whether the supervised token  $y_t$  is removed from the preservation set

Table 17: **Ablation results for LP-SFT design choices on Qwen3-4B trained with UltraFeedback.** We ablate three design factors: removing the supervised token  $y_t$  from the preservation set  $\mathcal{A}_t$ , using normalized probabilities to compute the KL loss, and applying the KL loss over either a local preservation set or the full vocabulary. Generation tasks are reported as pass@1 / pass@ $k$ ; MMLU is 5-shot accuracy. Avg. is the mean of all displayed scores in each row.

$\mu$	Remove $y_t$	Normalized KL	KL Scope	Math				Code				GEN.	Avg. All
				MATH-500		AIME 23-26		MBPP+		HE+		MMLU	
				pass@1 / pass@16	pass@1 / pass@32	pass@1 / pass@10	pass@1 / pass@10	pass@1 / pass@10	pass@1 / pass@10	5-shot Acc.			
1.0	No	Yes	Local	21.55	69.80	1.20	15.83	47.90	73.30	59.90	85.80	69.99	49.47
1.0	Yes	No	Local	21.36	70.40	0.96	10.83	46.70	74.60	59.10	<b>87.60</b>	70.28	49.09
1.0	No	No	Local	22.71	69.20	1.25	12.50	48.90	73.20	61.20	86.60	70.35	49.55
0.05	No	Yes	Local	36.83	72.60	1.95	13.33	46.70	67.90	58.40	84.60	69.13	50.16
0.05	Yes	No	Local	36.30	72.80	1.90	17.50	46.90	69.80	58.40	84.10	69.08	50.75
0.05	No	No	Local	37.16	74.40	1.98	19.17	46.20	67.50	57.90	84.60	69.14	50.89
1.0	Yes	Yes	Full	<b>44.31</b>	76.00	<b>2.76</b>	16.67	52.60	77.80	63.84	87.50	<b>70.47</b>	54.66
1.0	Yes	Yes	Local	42.79	76.80	2.47	<b>20.83</b>	51.60	76.49	<b>64.42</b>	86.91	70.32	<b>54.74</b>

$\mathcal{A}_t$ , whether the KL loss is computed over normalized probabilities, and whether the KL constraint is applied locally or over the full vocabulary.

The first group of variants shows that removing either target-token removal or local KL normalization substantially weakens the method. When  $y_t$  is kept in the preservation set, the preservation loss can directly compete with the cross-entropy objective. When local normalization is removed, the KL term is affected by absolute probability mass rather than focusing on relative preferences among non-label alternatives. Both cases lead to much lower average performance than the full LP-SFT design. The comparison between  $\mu = 1.0$  and  $\mu = 0.05$  further shows that these incomplete variants are sensitive to the preservation weight, suggesting that the two components are important for stable optimization.

**Local versus full-vocabulary preservation.** Table 17 also compares local preservation with a full non-label vocabulary KL variant that removes  $y_t$  and uses normalized probabilities. The full-vocabulary variant achieves competitive performance, especially on MBPP+ and MMLU, indicating that preserving base-model preferences can help retain general capabilities. However, the local variant achieves a slightly higher overall average while improving AIME and HE+ performance. This suggests that local preservation captures much of the benefit of full-vocabulary anchoring, while avoiding unnecessary constraints on the entire predictive distribution.

**Support schedule.** Table 18 further compares different choices of  $k_t$  on UltraFeedback across three backbone models. The main LP-SFT variant uses the  $N_1$ -adaptive support schedule,  $k_t = \min(\lceil N_1(q_t) \rceil, K_{\max})$ . We additionally evaluate a fixed upper-envelope schedule that uses  $k_t = K_{\max} = 10$  for all token positions. This variant uses the same target-token removal and local KL normalization as LP-SFT, and differs only in the support schedule. Fixed top-10 performs better on Qwen3-4B and Qwen3-14B, but is slightly worse on Llama3.1-8B, suggesting that the choice of  $k_t$  may depend on the quality of the base model distribution.

Overall, the ablation confirms that the effectiveness of LP-SFT comes from the combination of target-token removal, normalized KL, and local preservation. These choices allow the method to preserve useful non-label structure while remaining compatible with cross-entropy learning on the supervised target token.

### E.3 Training Efficiency and Cost

Table 19 compares the training time and peak memory usage of different SFT objectives. For LP-SFT, we report the cost of the fine-tuning stage and exclude the offline base-model precomputation time. This precomputation is a one-time data preprocessing step, performed together with the construction of tokenized training caches, and the cached base logits can be reused across different fine-tuning runs and ablation variants. While the precomputation requires one frozen-base forward pass and therefore scales with model size, it is amortized over subsequent runs and does not affect the peak memory usage during fine-tuning.

Since LP-SFT only applies a lightweight local KL loss over small adaptive supports during training, it introduces modest overhead compared with standard CE. In contrast, ASFT requires running an additional base model

Table 18: **Support-schedule comparison on UltraFeedback.** We compare the default  $N_1$ -adaptive schedule with a fixed top-10 schedule across three backbone models. Generation tasks are reported as pass@1/pass@ $k$ ; MMLU is 5-shot accuracy. Avg. is the mean of all displayed scores in each row.

Model	Schedule	Math				Code				GEN.	Avg.
		MATH-500		AIME 23-26		MBPP+		HE+		MMLU	All
		pass@1 / pass@16	pass@1 / pass@16	pass@1 / pass@32	pass@1 / pass@32	pass@1 / pass@10	pass@1 / pass@10	pass@1 / pass@10	pass@1 / pass@10	5-shot Acc.	
Qwen3-4B	Fixed top-10	<b>44.11</b>	<b>77.60</b>	2.40	<b>20.83</b>	<b>53.30</b>	<b>78.50</b>	64.30	<b>87.30</b>	<b>70.43</b>	<b>55.42</b>
	$N_1$ -Adaptive	42.79	76.80	<b>2.47</b>	<b>20.83</b>	51.60	76.49	<b>64.42</b>	86.91	70.32	54.74
Llama3.1-8B	Fixed top-10	7.86	37.00	0.05	1.67	36.10	61.60	29.10	57.60	<b>62.71</b>	32.63
	$N_1$ -Adaptive	<b>8.48</b>	<b>40.00</b>	<b>0.10</b>	<b>3.33</b>	<b>37.94</b>	<b>63.95</b>	<b>30.18</b>	<b>59.60</b>	62.48	<b>34.01</b>
Qwen3-14B	Fixed top-10	<b>47.05</b>	<b>80.00</b>	<b>3.15</b>	<b>19.17</b>	<b>66.60</b>	84.19	71.25	88.82	<b>78.93</b>	<b>59.91</b>
	$N_1$ -Adaptive	45.19	77.80	2.71	18.33	65.90	<b>84.34</b>	<b>72.13</b>	<b>90.16</b>	78.82	59.49

during training and applies a full-vocabulary KL constraint, leading to substantially higher training time and memory usage.

Table 19: **Training efficiency and cost comparison.** Results are measured on Qwen3-4B. Time and memory are reported relative to standard CE training.

Method	Time Ratio	Peak Memory Ratio
CE	1.00×	1.00×
DFT	1.00×	0.87×
EAFT	1.02×	1.22×
GEM	1.01×	1.01×
ASFT	1.33×	1.47×
LP-SFT	1.07×	1.10×